Journal of Materials Chemistry C

PAPER

View Article Online
View Journal | View Issue

Cite this: J. Mater. Chem. C, 2018, 6, 9453

Asymmetric tris-heteroleptic iridium(III) complexes containing three different 2-phenylpyridine-type ligands: a new strategy for improving the electroluminescence ability of phosphorescent emitters†

Wanping Dang,[a] Xiaolong Yang,[a] Zhao Feng,[a] Yuanhui Sun,[a] Daokun Zhong,[a] Guijiang Zhou,*[a] Zhaoxin Wu*[b] and Wai-Yeung Wong*[c]

A series of asymmetric tris-heteroleptic Ir(III) phosphorescent complexes adopting both IrLL′L″ (**Ir3-1** and **Ir3-2**) and IrLL′(acac) (**Ir2-1** and **Ir2-2**) chemical constitution have been successfully prepared, where L, L′ and L″ represent different ppy-type (2-phenylpyridine) ligands. The IrLL′L″ asymmetric tris-heteroleptic Ir(III) phosphorescent complexes **Ir3-1** and **Ir3-2** bearing three different ppy-type ligands can show better thermal stability, higher Φ_P and improved ability of trapping both holes and electrons than IrLL′(acac) asymmetric analogs **Ir2-1** and **Ir2-2**. Thanks to these advantages, **Ir3-1** and **Ir3-2**, especially **Ir3-2**, can show phenomenal EL performance with a maximum external quantum efficiency (η_{ext}) of 26.2%, a maximum current efficiency (η_L) of 88.7 cd A^{-1} and a maximum power efficiency (η_P) of 75.3 lm W^{-1}, much higher than the data achieved by not only IrLL′(acac) asymmetric analogs **Ir2-1** and **Ir2-2**, but also the traditional $Ir(L)_3$ symmetric counterparts. To the best of our knowledge, these data represent the highest EL efficiencies ever achieved by the asymmetric ppy-type Ir(III) phosphorescent complexes reported in the literature. All these encouraging results not only indicate the great potential of the unique asymmetric IrLL′L″ structures bearing three different ppy-type ligands in improving the EL ability of ppy-type Ir(III) phosphorescent emitters, but also represent important progress in the design and synthesis of new asymmetric ppy-type Ir(III) phosphorescent complexes with high EL ability.

Received 15th June 2018,
Accepted 5th August 2018

DOI: 10.1039/c8tc02940g

rsc.li/materials-c

Introduction

Owing to their strong phosphorescence, relatively short lifetime of excited states and tunable emission color, 2-phenylpyridine (ppy)-type Ir(III) complexes have drawn substantial attention from both academic and industrial communities involving electroluminescence (EL).[1–7] The EL devices *i.e.* organic light-emitting diodes (OLEDs) can fulfill high efficiencies with these ppy-type Ir(III) complexes as emitters. One of the merits associated with ppy-type Ir(III) complexes is the versatile tuning of photophysical properties through changing the chemical structures of ppy-type ligands,[8–12] definitely representing a key feature to furnish their great success in the field of EL. Typically, the emission color, charge carrier injection/transporting ability, and phosphorescent quantum yield (Φ_P) of the ppy-type Ir(III) complexes can be easily tuned by their ppy-type ligands.[1,7,13–20] Generally, the phosphorescent ppy-type Ir(III) complexes adopt two types of chemical constitution: IrLL′L″ and IrLL′(acac) (acac: acetylacetone anion). Hence, multiple ppy-type ligands in a single complex molecule can provide a wide scope to optimize the properties of the concerned ppy-type Ir(III) complexes.

Recently, novel Ir(III) complexes with IrLL′(acac) chemical constitution have been developed with two different ppy-type ligands.[7,19,21–25] Encouragingly, these asymmetric tris-heteroleptic Ir(III) complexes can show tuned emission color and greatly

[a] MOE Key Laboratory for Nonequilibrium Synthesis and Modulation of Condensed Matter, State Key Laboratory for Mechanical Behavior of Materials, Department of Chemistry, School of Science, Xi'an Jiaotong University, Xi'an 710049, P. R. China. E-mail: zhougj@mail.xjtu.edu.cn; Fax: +86-29-8266-3914
[b] Key Laboratory for Physical Electronics and Devices of the Ministry of Education, Faculty of Electronic and Information Engineering, Xi'an Jiaotong University, Xi'an 710049, P. R. China. E-mail: zhaoxinwu@mail.xjtu.edu.cn
[c] Department of Applied Biology and Chemical Technology, The Hong Kong Polytechnic University, Hung Hom, Hong Kong, P. R. China. E-mail: wai-yeung.wong@polyu.edu.hk

† Electronic supplementary information (ESI) available: Synthetic scheme and procedure of the organic ligands, ^1H and ^{13}C NMR spectra; TGA curves, PL spectra in PMMA film and at 77 K for the asymmetric tris-heteroleptic Ir(III) phosphorescent complexes, and EL results for the devices except for the optimized ones. See DOI: 10.1039/c8tc02940g

enhanced EL efficiencies, indicating the great potential of employing different ppy-type ligands in a single molecule of the Ir(III) complexes. IrLL′L″ phosphorescent complexes with different ppy-type ligands have been reported as well.[26–30] However, they typically adopt two ppy-type ligands with the same chemical structure which is different from that of the third ppy-type ligand. Derosa and co-workers[27] reported that the Φ_P of complex *fac*-Ir(ppy)$_2$(vppy) is much larger than that of complex Ir(ppy)$_2$(vacac) (*e.g.* Φ_P = 0.20 for *fac*-Ir(ppy)$_2$(vppy) and Φ_P = 0.02 for Ir(ppy)$_2$(vacac)). Burn and co-workers[29] found that an Ir(III) complex with two different kinds of ppy-type ligands shows better EL properties (η_{ext} = 5.7% and η_P = 4.5 lm W^{-1}) than its counterpart possessing only one kind of ppy-type-ligand (η_{ext} = 4.25% and η_P = 1.00 lm W^{-1}). Park's group[30] synthesized red phosphorescent Ir(III) complexes Ir(ppy)$_2$(dpq-3F) and Ir(dpq-3F)$_3$ and used them as emitters to fabricate OLEDs, which also showed that introducing different kinds of ligands to the complexes could effectively enhance the EL efficiencies of the devices (η_L = 13.70 cd A^{-1}, η_P = 10.80 lm W^{-1} for Ir(ppy)$_2$(dpq-3F) and η_L = 8.17 cd A^{-1}, η_P = 7.33 lm W^{-1} for Ir(dpq-3F)$_3$). Clearly, there should be a chance to optimize the EL ability of the IrLL′L″ phosphorescent complexes by employing three different ppy-type ligands in a single complex molecule.[31–34] Recently, Tamura and co-workers[33] reported different stereoisomers of tris-heteroleptic tris-cyclometalated Ir(III) complexes showing different photophysical properties; however, the study of the EL properties of these Ir(III) complexes has not been further explored.

Bearing this in mind, two novel IrLL′L″ phosphorescent complexes have been successfully developed with three different ppy-type ligands chelated with an Ir(III) center. In addition, based on the success achieved by the functional groups attached to the ppy-type Ir(III) phosphorescent complexes, diphenylamino-fluorenyl and phenylsulfonyl groups have been introduced to the tris-heteroleptic IrLL′L″ phosphorescent complexes. Encouragingly, both thermal and EL performances have been noticeably improved. This research should represent a new outlet for the design and optimization of the EL performances of ppy-type Ir(III) phosphorescent complexes.

Experimental

General information

Commercially available chemicals were used directly for synthesis without further purification. All solvents for the reactions were dried and distilled prior to use. The reactions were monitored using thin layer chromatography (TLC) purchased from Merck & Co., Inc. Flash column chromatography and preparative TLC plates were made with silica gel from Shenghai Qingdao (300–400 mesh). ^{1}H and ^{13}C spectra were recorded in $CDCl_3$ on a Bruker Avance 400 MHz spectrometer. Chemical shifts were quoted to the solvent residual peak at δ 7.26 ppm for ^{1}H and 77.00 ppm for ^{13}C NMR spectra, respectively. UV-vis absorption spectra were recorded on a Perkin Elmer Lambda 950 spectrophotometer. Emission spectra and lifetimes of these complexes were recorded on an Edinburgh Instruments, Ltd. (FLSP920) fluorescence spectrophotometer. Phosphorescence quantum yields (Φ_P) were measured in CH_2Cl_2 solution against *fac*-[Ir(ppy)$_3$] (Φ_P = 0.97) standard at 293 K.[35] The thermal gravimetric analysis (TGA) and differential scanning calorimetry (DSC) data were obtained on a NETZSCH STA 409 C instrument and a NETZSCH DSC 200 PC unit, respectively. Cyclic voltammetry (CV) measurements were performed with a Princeton Applied Research model 273A potentiostat with 100 mV s^{-1} scan rate. All the CV experiments were carried out in a three-electrode compartment cell with a Pt-sheet counter electrode, a glassy carbon working electrode and a Ag/AgCl reference electrode. The supporting electrolyte was a 0.1 M acetonitrile solution of [*n*Bu$_4$N]BF$_4$, containing ferrocene as the internal reference. The data of elemental analyses were obtained on a Flash EA 1112 elemental analyzer. Fast atom bombardment (FAB) mass spectra were recorded on a Finnigan MAT SSQ710 system.

Synthesis

All the ppy-type organic ligands were prepared according to our previously published procedures.[36–38] The synthetic details have been provided in the ESI.†

General procedure for the synthesis of Ir3-1 and Ir3-2

To a mixed solution of 2-ethoxyethanol and H_2O (3 : 1, v/v), **L1**/**L2** (1.1 equiv.), **L3** (1.1 equiv.), and $IrCl_3{\cdot}nH_2O$ (1.0 equiv., 60 wt% Ir content) were added under a nitrogen atmosphere. The reaction mixture was allowed to stir at 110 °C for 16 h. After cooling to room temperature, saturated NaCl solution was added to the reaction mixture and the colored Ir(III) μ-chloro-bridged dimer formed was collected by filtration. Subsequently, after drying, the Ir(III) μ-chloro-bridged dimer (1.0 equiv.), CF_3SO_3Ag (2.0 equiv.) and 2-phenylpyridine (3.0 equiv.) were added to acetone. The reaction mixture was allowed to react at 80 °C for 16 h. After cooling to room temperature, the white solid was removed and the residue was purified on preparative TLC plates with CH_2Cl_2/hexane (3 : 1) as the eluent.

Ir3-1. Yield: 10.7%. ^{1}H NMR (400 MHz, $CDCl_3$): δ (ppm) 7.90–7.84 (m, 3H), 7.68 (d, J = 8.0 Hz, 1H), 7.63–7.56 (m, 9H), 7.49 (dd, J = 4.0, 1.6 Hz, 1H), 7.43 (d, J = 5.2 Hz, 1H), 7.40–7.35 (m, 2H), 7.25–7.17 (m, 7H), 7.08 (d, J = 8.0 Hz, 5H), 6.98–6.94 (m, 4H), 6.88–6.84 (m, 3H), 6.81 (t, J = 6.0 Hz, 1H), 6.63 (t, J = 7.0 Hz, 1H), 6.35 (d, J = 7.6 Hz, 1H), 1.94–1.87 (m, 4H), 0.57 (t, J = 8.0 Hz, 3H), 0.34 (t, J = 8.0 Hz, 3H). ^{13}C NMR (100 MHz, $CDCl_3$): δ (ppm) 166.72, 166.67, 164.93, 162.87, 160.51, 157.98, 152.37, 148.63, 148.08, 147.45, 147.04, 146.82, 146.78, 143.68, 142.76, 142.27, 141.83, 140.76, 137.45, 137.03, 136.18, 136.01, 132.12, 129.70, 129.04, 128.61, 127.37, 126.91, 123.98, 123.69, 123.61, 123.46, 122.11, 121.83, 121.24, 120.75, 119.96, 119.89, 119.67, 119.02, 118.95, 118.46, 118.29, 33.30, 32.78, 8.89, 8.77; FAB-MS (m/z): 1106 [M]$^+$; anal. calcd for $C_{62}H_{49}IrN_4O_2S$: C, 67.31; H, 4.46; N, 5.06; found: C, 67.22; H, 4.38; N. 4.92%.

Ir3-2. Yield: 18.2%. ^{1}H NMR (400 MHz, $CDCl_3$): δ (ppm) 7.88 (d, J = 8.0 Hz, 1H), 7.84 (t, J = 8.0 Hz, 2H), 7.67 (d, J = 8.0 Hz, 1H), 7.63–7.53 (m, 9H), 7.49 (dd, J = 4.4, 1.8 Hz, 1H), 7.41 (d, J = 5.6 Hz, 1H), 7.38–7.36 (m, 2H), 7.22 (t, J = 6.0 Hz, 2H), 7.11

(d, J = 8.0 Hz, 1H), 7.02 (d, J = 9.2 Hz, 4H), 6.96–6.94 (m, 2H), 6.86–6.77 (m, 9H), 6.61 (t, J = 7.4 Hz, 1H), 6.33 (d, J = 8.0 Hz, 1H), 3.79 (s, 6H), 2.05–1.79 (m, 4H), 0.57 (t, J = 8.0 Hz, 3H), 0.34 (t, J = 8.0 Hz, 3H). ^{13}C NMR (100 MHz, $CDCl_3$): δ (ppm) 166.82, 166.70, 164.97, 160.63, 157.96, 155.16, 152.24, 148.63, 147.93, 147.47, 147.06, 146.76, 143.71, 143.53, 142.79, 142.10, 141.78, 141.38, 140.81, 137.05, 136.18, 136.09, 136.01, 135.76, 132.13, 129.68, 128.66, 127.40, 126.62, 125.49, 123.98, 123.61, 123.42, 121.84, 121.09, 120.52, 119.93, 119.90, 119.02, 118.88, 118.47, 118.24, 117.01, 114.49, 55.51, 55.34, 33.33, 32.82, 8.94, 8.81; FAB-MS (m/z): 828 $[M]^+$; FAB-MS (m/z): 1166 $[M]^+$; anal. calcd for $C_{64}H_{53}IrN_4O_4S$: C, 65.90; H, 4.58; N, 4.80; found: C, 65.81; H, 4.49; N. 4.72%.

General procedure for the synthesis of Ir2-1 and Ir2-2

To the dry CH_2Cl_2, *t*BuOK (2.5 equiv.) and acetylacetone (3.0 equiv.) were added and the mixture was stirred for 30 min at room temperature. Then, the Ir(III) μ-chloro-bridged dimer (1.0 equiv.) was added. The reaction mixture was stirred at room temperature for 6 h. Then water was added to the reaction mixture. The mixture was extracted with CH_2Cl_2 and the combined organic phase was dried over $MgSO_4$. The solvent was removed under reduced pressure and the residue was purified on preparative TLC plates with CH_2Cl_2/ethyl acetate (30 : 1) as the eluent.

Ir2-1. Yield: 22.7%. ^{1}H NMR (400 MHz, $CDCl_3$): δ (ppm) 8.64 (d, J = 8.0 Hz, 1H), 8.44 (d, J = 4.0 Hz, 1H), 7.89 (t, J = 8.0 Hz, 2H), 7.82–7.76 (m, 2H), 7.59 (t, J = 8.0 Hz, 3H), 7.42 (s, 1H), 7.39 (d, J = 8.0 Hz, 1H), 7.31–7.27 (m, 4H), 7.19 (t, J = 8.0 Hz, 5H), 7.07 (d, J = 8.0 Hz, 1H), 7.03 (d, J = 8.0 Hz, 4H), 6.96 (t, J = 7.4 Hz, 3H), 6.83 (dd, J = 4.1, 1.8 Hz, 1H), 6.73 (d, J = 1.6 Hz, 1H), 6.34 (s, 1H), 5.25 (s, 1H), 1.89–1.79 (m, 10H), 0.37 (t, J = 8.0 Hz, 3H), 0.19 (t, J = 8.0 Hz, 3H). ^{13}C NMR (100 MHz, $CDCl_3$): δ (ppm) 184.85, 184.79, 168.32, 166.93, 152.27, 150.00, 148.78, 148.17, 147.95, 146.98, 144.69, 142.91, 142.59, 142.16, 142.04, 139.49, 137.15, 136.43, 132.40, 131.00, 129.07, 128.71, 127.34, 123.83, 123.60, 123.42, 123.09, 122.97, 122.29, 121.20, 120.34, 119.62, 119.38, 118.57, 118.21, 100.55, 55.23, 32.85, 32.73, 28.73, 8.84; FAB-MS (m/z): 1051 $[M]^+$; anal. calcd for $C_{56}H_{48}IrN_3O_4S$: C, 63.98; H, 4.60; N, 4.00; found: C, 63.88; H, 4.51; N. 3.91%.

Ir2-2. Yield: 21.5%. ^{1}H NMR (400 MHz, $CDCl_3$): δ (ppm) 8.63 (d, J = 4.0 Hz, 1H), 8.42 (d, J = 8.0 Hz, 1H), 7.87 (d, J = 8.0 Hz, 2H), 7.81–7.77 (m, 2H), 7.58 (t, J = 8.0 Hz, 3H), 7.39 (t, J = 7.4 Hz, 2H), 7.30–7.27 (m, 3H), 7.25 (s, 1H), 7.14 (t, J = 6.8 Hz, 1H), 7.01–6.94 (m, 5H), 6.85 (d, J = 8.0 Hz, 1H), 6.77 (d, J = 8.0 Hz, 4H), 6.72–6.69 (m, 2H), 6.29 (s, 1H), 5.24 (s, 1H), 3.78 (s, 6H), 1.87–1.76 (m, 10H), 0.36 (t, J = 8.0 Hz, 3H), 0.18 (t, J = 8.0 Hz, 3H). ^{13}C NMR (100 MHz, $CDCl_3$): δ (ppm) 184.79, 168.36, 166.90, 155.26, 152.10, 149.98, 149.42, 148.76, 148.10, 148.02, 144.60, 142.65, 142.44, 142.03, 141.49, 139.43, 137.06, 134.59, 132.34, 130.98, 128.67, 127.30, 125.62, 123.77, 122.91, 122.74, 120.99, 120.63, 120.05, 119.55, 118.42, 118.15, 116.50, 114.46, 100.50, 55.08, 53.42, 32.83, 32.69, 28.70, 8.83; FAB-MS (m/z): 1111 $[M]^+$; anal. calcd for $C_{58}H_{52}IrN_3O_6S$: C, 62.68; H, 4.72; N, 3.78; found: C, 62.56; H, 4.63; N. 3.65%.

Computational details

DFT calculations using B3LYP were performed for all of the iridium(III) complexes. The basis set used for C, H, N, O, and S atoms was 6-31G(d,p), while effective core potentials with a LanL2DZ basis set were employed for Ir atoms.[39,40] Excitation behaviors were obtained using TD-DFT calculations based on the optimized ground state geometries. In addition, UB3LYP was used to optimize the first triplet state (T_1) geometries and the natural transition orbital (NTO) was analyzed for $S_0 \rightarrow T_1$ excitation. All the calculations were carried out by using the Gaussian 09 program.[41]

Results and discussion

Synthesis and structural characterization

Synthetic protocols of all the asymmetric ppy-type Ir(III) phosphorescent complexes with different chemical constitution are shown in Scheme 1. The key μ-chloro-bridged complex was prepared by cyclometalation of $IrCl_3{\cdot}nH_2O$ (Ir 60.0 wt%) by **L1** or **L2** and **L3** in a mixture of 2-ethoxyethanol and water (3 : 1, v/v). For the synthesis of complexes **Ir3-1** and **Ir3-2**, the μ-chloro-bridged complex can be treated with 2-phenylpyridine (ppy) and CF_3SO_3Ag in acetone at 80 °C. By adding the μ-chloro-bridged complex in a mixture of acetylacetone and *t*BuOK, complexes **Ir2-1** and **Ir2-2** can be obtained. The electronically active diphenylamine and sulfonyl groups have been attached to the ppy-type ligands to furnish the charge carrier injection/transporting ability to all the complexes. Unexpectedly, *fac*-isomers for **Ir3-1** and **Ir3-2** have been obtained, since *mer*-isomers should be typically formed in this synthetic strategy at a low reaction temperature (*ca.* 80 °C).[27]

The facial configuration of **Ir3-1** and **Ir3-2** has been confirmed by their ^{1}H-NMR spectra, in which the chemical shifts for the three protons on the C atoms adjacent to N atoms in the pyridyl rings of three ppy-type ligands located at *ca.* 7.9 ppm (Fig. S1a and S1b in the ESI†). However, the same protons in the meridianal isomers typically give resonance peaks in a much lower field of *ca.* 9.0 ppm.[27,33] The resonance peaks at *ca.* 2.0 ppm together with the two sets of triplet peaks at *ca.* 0.6 and 0.3 ppm can be assigned to the protons from the two ethyl groups on the fluorene unit in **Ir3-1** and **Ir3-2** (Fig. S1a and S1b in the ESI†). In the ^{1}H-NMR spectra of **Ir2-1** and **Ir2-2**, the two sets of doublet peaks at *ca.* 8.6 and 8.4 ppm can be assigned to the two protons on the C atoms adjacent to N atoms in the pyridyl rings of two ppy-type ligands, respectively (Fig. S1c and S1d in the ESI†). The single peak at *ca.* 3.8 ppm has been induced by the methoxyl groups in both **Ir3-2** and **Ir2-2** (Fig. S1b and S1d in the ESI†). The auxiliary ligand acetylacetone anion in **Ir2-1** and **Ir2-2** can be indicated by the signals at *ca.* 5.3 and 1.8 ppm, respectively (Fig. S1c and S1d in the ESI†). All these spectral data have clearly indicated the proposed chemical structures of these asymmetrical Ir(III) complexes.

Thermal and photophysical properties

Under nitrogen flow, thermal properties of these asymmetric tris-heteroleptic Ir(III) complexes have been characterized by

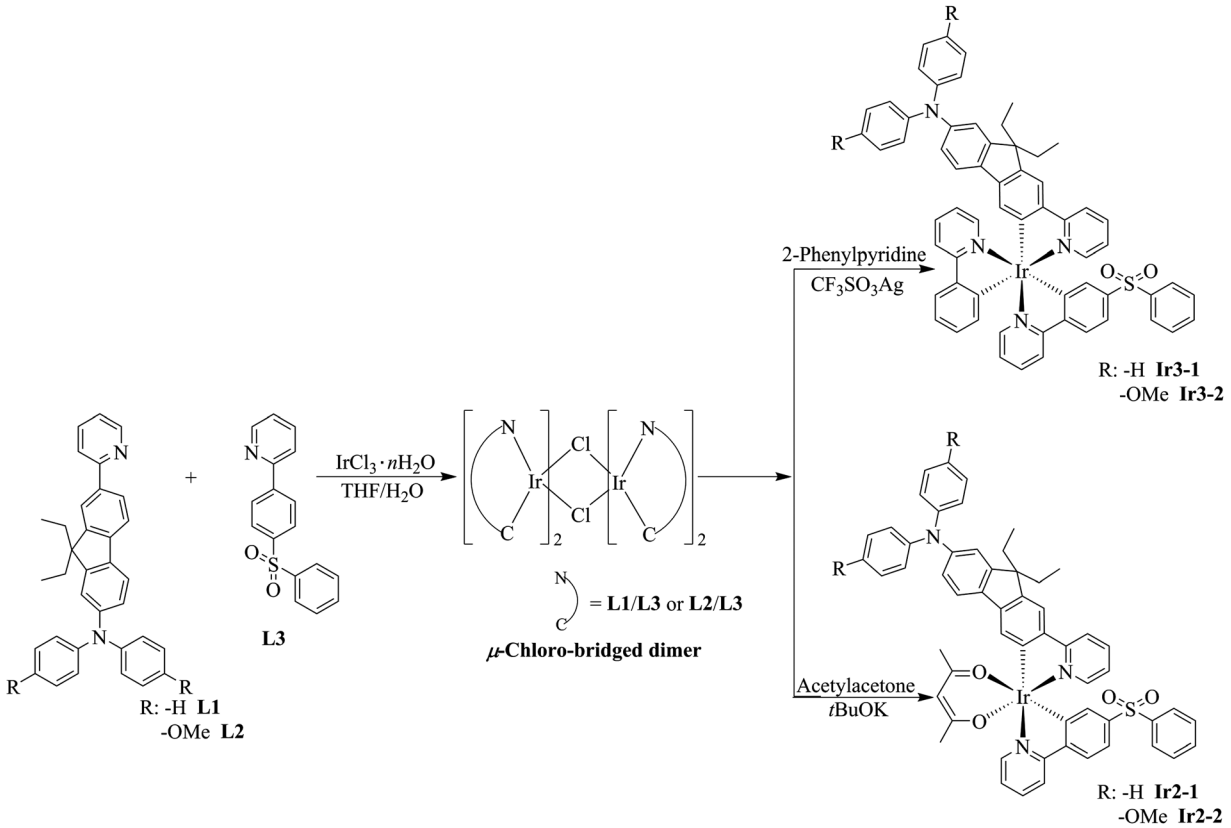

Scheme 1 Synthetic scheme for the iridium(III) complexes.

thermogravimetric analysis (TGA) and different scanning calorimetry (DSC). The TGA results reveal the obvious difference in the thermal stability of these tris-heteroleptic Ir(III) complexes. Complexes **Ir3-1** and **Ir3-2** bearing three ppy-type ligands can show noticeably higher 5% weight-reduction temperature ($\Delta T_{5\%}$, *ca.* 390 °C for **Ir3-1** and 387 °C for **Ir3-2**) than that of **Ir2-1** and **Ir2-2** (*ca.* 369 °C and 343 °C, respectively) with the acetylacetone anion auxiliary ligand (Table 1 and Fig. S2 in the ESI†). The $\Delta T_{5\%}$ data can be explained by the coordinate covalent bond length between the Ir atom and ppy or acac ligands based on TD-DFT calculations. The bond length of Ir–C (2.02865 Å for **Ir3-1** and 2.02817 Å for **Ir3-2**) and Ir–N (2.18316 Å for **Ir3-1** and 2.18394 Å for **Ir3-2**) are shorter than Ir–O bonds (*ca.* 2.20 Å) (Table S1 in the ESI†). So, **Ir3-1** and **Ir3-2** should show higher decomposition temperatures than **Ir2-1** and **Ir2-2**. This conclusion had been confirmed by our previous studies as well.[8,38] Furthermore, the DSC traces have indicated that **Ir3-1** and **Ir3-2** can show higher glass-transition temperatures (T_g, *ca.* 135 °C for **Ir3-1** and 130 °C for **Ir3-2**) than **Ir2-1** (*ca.* 125 °C) and **Ir2-2** (*ca.* 123 °C) (Table 1). In our previous results, the DSC data indicated that the complex with three identical ppy-type ligands functionalized with the diphenylamine group showed a slight difference in T_g compared with the analog bearing an acac auxiliary ligand (157 °C and 160 °C, respectively).[8,38] The results suggest that T_g is closely related to the rotational functional groups attached to the ppy-type ligands, such as diphenylamine and phenylsulfonyl in **L1**, **L2** and **L3**. However, ppy and acac ligands can form highly rigid

Table 1 Photophysical and thermal data of the asymmetric tris-heteroleptic Ir(III) complexes

Compound	Absorption λ_{abs}[a] (nm) 298 K	Emission λ_{em}[a] (nm) solution 293 K/77 K	Φ_P solution[b]/film[c] 293 K	τ_P solution[d]/film[e] (μs) 293 K	$\Delta T_{5\%}/T_g$ (°C)	E_T[f]/(eV) 293 K
Ir3-1	289 (4.85), 383 (4.60), 402 (4.61), 459 (3.96)	562, 615/562, 610	0.41/0.78	0.14/2.52	390/135	2.21
Ir3-2	291 (4.88), 409 (4.67), 456 (4.20)	566, 616/567, 612	0.28/0.76	0.12/2.98	387/130	2.19
Ir2-1	259 (4.71), 285 (4.81), 384 (4.61), 399 (4.61), 458 (4.08)	568, 622/570, 616	0.33/0.57	0.24/3.36	369/125	2.18
Ir2-2	260 (4.67), 287 (4.75), 408 (4.55), 457 (4.24)	575, 625/577, 618	0.20/0.58	0.17/3.08	343/123	2.16

[a] Measured in CH_2Cl_2 at a concentration of 10^{-5} M and log ε values are shown in parentheses. [b] In relative to *fac*-[Ir(ppy)$_3$] (Φ_p = 0.97%), λ_{ex} = 360 nm. [c] Doped PMMA film of the 6 wt% doping-level with a thickness of *ca.* 200 nm on quartz. Measured in an integrating sphere, λ_{ex} = 360 nm. [d] Measured in degassed CH_2Cl_2 at a concentration of 10^{-5} M. [e] Measured in doped PMMA film of 6 wt% doping-level with a thickness of *ca.* 200 nm on quartz, λ_{ex} = 360 nm. [f] E_T represents the triplet energy level.

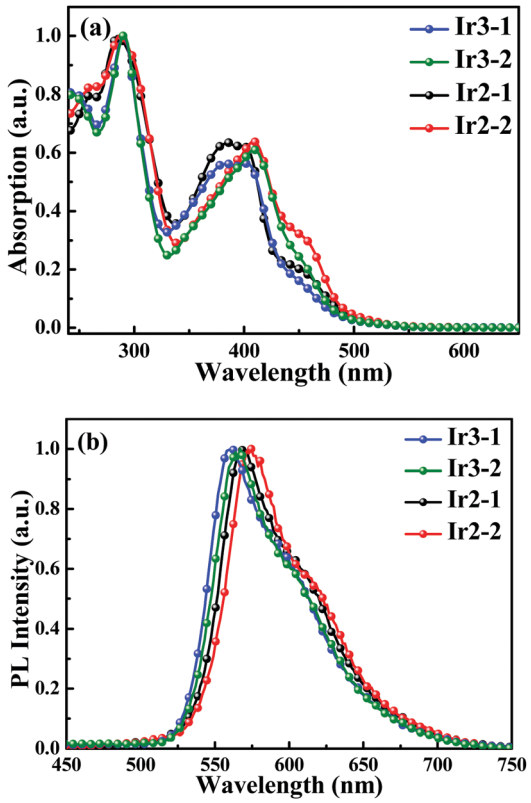

Fig. 1 (a) UV-vis absorption spectra and (b) photoluminescence (PL) spectra of the asymmetric tris-heteroleptic Ir(III) complexes in CH_2Cl_2 solution recorded at 293 K.

structures after being coordinated with the Ir center, showing negligible influence on the T_g. Clearly, all these complexes possess diphenylamine and phenylsulfonyl groups, furnishing their similar T_gs. All these data have indicated the advantage of tris-heteroleptic Ir(III) complexes with *fac*-IrLL′L″ chemical constitution in maintaining enhanced thermal properties which should benefit their application in OLEDs.

In their UV-vis spectra (Fig. 1a), the high-energy absorption bands before *ca.* 430 nm can be safely assigned to the π–π* transition of the ppy-type ligands and the weak low-energy absorption bands after 430 nm can be ascribed to the triplet absorption band.[13,19,21,22] According to time-dependent density functional theory (TD-DFT) calculations, the $S_0 \rightarrow S_1$ transition characteristics of these asymmetric tris-heteroleptic Ir(III) complexes can be represented by their HOMO → LUMO (H → L) transitions due to their large contribution over 80% (Table 2). It is well accepted that $S_0 \rightarrow S_1$ transition can correspond to the major absorption bands.[21,22] Hence, the H → L transition patterns of these asymmetric tris-heteroleptic Ir(III) complexes can be employed to interpret their absorption behaviors. Based on the H → L transition features of these asymmetric tris-heteroleptic Ir(III) complexes, their major absorption bands centered at *ca.* 400 nm should exhibit the ligand-to-ligand charge transfer (LLCT) feature from the π orbitals of the diphenylaminofluorene unit in the ppy-type ligands **L1**/**L2** to the π* orbitals of **L3**, especially the π* orbitals of the pyridyl unit **L3** (Fig. 2). Their high-energy absorption bands before 300 nm should be induced by the π–π* transitions associated with the small aromatic units in the ppy-type ligands. Based on the TD-DFT results in Table 2, the feature of the triplet

Table 2 TD-DFT results for these asymmetric tris-heteroleptic Ir(III) complexes based on their optimized S_0 geometries

Complexes	MO	Contribution percentages of metal d_π orbitals and π orbitals of ligands to MOs/%				Main configuration of $S_0 \rightarrow S_1$ excitation/E_{cal}/λ_{cal}/f[a]	Main configuration of $S_0 \rightarrow T_1$ excitation/E_{cal}/λ_{cal}[a]
Ir3-1		**Ir**	**L1**	**L3**	**ppy**	H → L (80.35%)	H → L (10.04%)
	L+1	2.95	87.45	5.73	3.87	H−1 → L (17.97%)	H → L+1 (60.86%)
	L	2.16	5.79	90.41	1.64	2.572 eV	H−1 → L+1 (5.97%)
	H	1.37	98.32	0.21	0.10	482.0 nm	2.224 eV
	H−1	44.09	35.26	5.25	15.40	f = 0.0329	557.6 nm
Ir3-2		**Ir**	**L2**	**L3**	**ppy**	H → L (95.78%)	H → L (10.94%)
	L+1	2.86	85.34	4.43	7.37	2.410 eV	H → L+1 (59.92%)
	L	2.24	4.30	91.90	1.54	514.5 nm	H−1 → L+1 (7.07%)
	H	0.46	99.41	0.09	0.04	f = 0.0311	2.149 eV
	H−1	41.23	44.48	4.66	9.63		576.9 nm
Ir2-1		**Ir**	**L1**	**L3**	**acac**	H → L (65.67%)	H → L (3.08%)
	L+1	3.09	94.90	1.32	0.69	H−1 → L (32.44%)	H → L+1 (70.18%)
	L	3.56	0.94	94.90	0.60	2.505 eV	H−1 → L+1 (6.43%)
	H	3.19	95.65	0.91	0.25	494.9 nm	2.221 eV
	H−1	38.98	39.00	17.70	4.32	f = 0.0129	558.1 nm
Ir2-2		**Ir**	**L2**	**L3**	**acac**	H → L (92.21%)	H → L (3.28%)
	L+1	3.21	94.79	1.27	0.73	2.373 eV	H → L+1 (68.30%)
	L	3.57	0.78	95.03	0.62	522.5 nm	H−1 → L+1 (9.11%)
	H	0.91	98.82	0.22	0.05	f = 0.0049	2.162 eV
	H−1	39.61	39.38	16.83	4.18		573.4 nm

[a] H → L represents the HOMO to LUMO transition. E_{cal}, λ_{cal} and f represent calculated excitation energy, calculated emission wavelength and oscillator strength, respectively. The oscillator strength of $S_0 \rightarrow T_1$ is zero due to the spin-forbidden nature of singlet–triplet transition using TD-DFT calculations in the Gaussian program without the consideration of spin–orbital coupling.

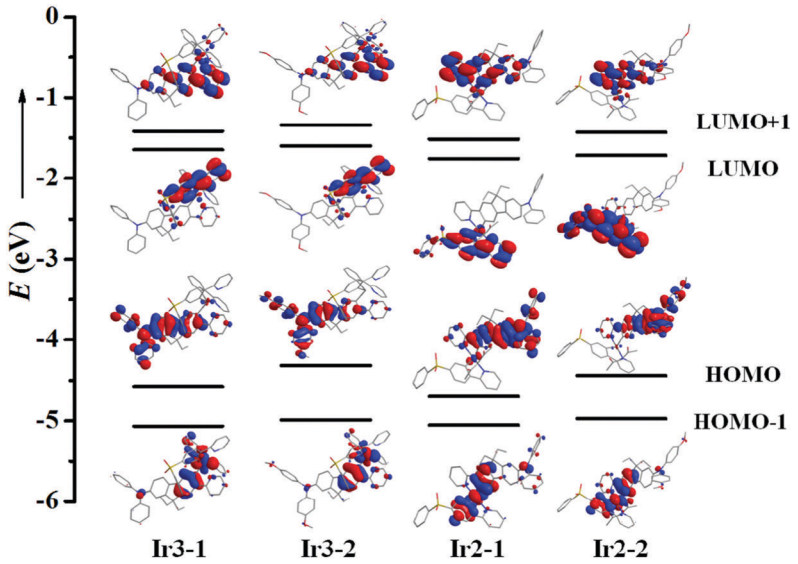

Fig. 2 Molecular orbital (MO) patterns (isocontour value = 0.030) of these asymmetric tris-heteroleptic Ir(III) complexes based on their optimized S_0 geometries.

absorption bands of these tris-heteroleptic Ir(III) complexes can be mainly represented by the H → L+1 transition. According to the MO patterns in Fig. 2, the triplet absorption bands of these tris-heteroleptic Ir(III) complexes can show the intra-molecular charge transfer (ILCT) feature in **L1**/**L2** together with slight metal-to-ligand charge transfer (MLCT) and LLCT characteristics.

Fig. 1b shows the photoluminescence(PL) spectra of these tris-heteroleptic Ir(III) complexes in CH_2Cl_2 solution at 293 K. Excited with 360 nm UV light, all of these tris-heteroleptic Ir(III) complexes emit an orange phosphorescent band at *ca.* 570 nm with weaker shoulder emission at *ca.* 620 nm (Fig. 1b and Table 1). Clearly, they can share very similar spectral line for their phosphorescence signals with a slightly different peak wavelength (Fig. 1b). In addition, their phosphorescent spectra can show a structured line profile (Fig. 1b), especially for the major emission bands in doped PMMA film (Fig. S3 in the ESI†) and at a low temperature of 77 K (Fig. S4 in the ESI†). In order to interpret the phosphorescent character *i.e.* the T_1 state character of these tris-heteroleptic Ir(III) complexes, natural transition orbitals (NTOs) have been obtained for their $S_0 \rightarrow T_1$ excitations with optimized T_1 geometries.

Based on the distribution patterns of the NTO hole and particle orbitals of all these asymmetric tris-heteroleptic Ir(III) complexes, they all display a prevailing ligand-centered feature for their $S_0 \rightarrow T_1$ excitation, centering on ligand **L1** or **L2** due to its large contribution to the NTOs (Fig. 3 and Table 3). This result can be ascribed to the electron-rich characteristics of the diphenylaminofluorene unit which should facilitate the electron transition process. So, the T_1 states of all the asymmetric tris-heteroleptic Ir(III) complexes show dominantly ligand-centered $^3\pi$–π^* features, which has been confirmed by the structured line profile of the major phosphorescent band in

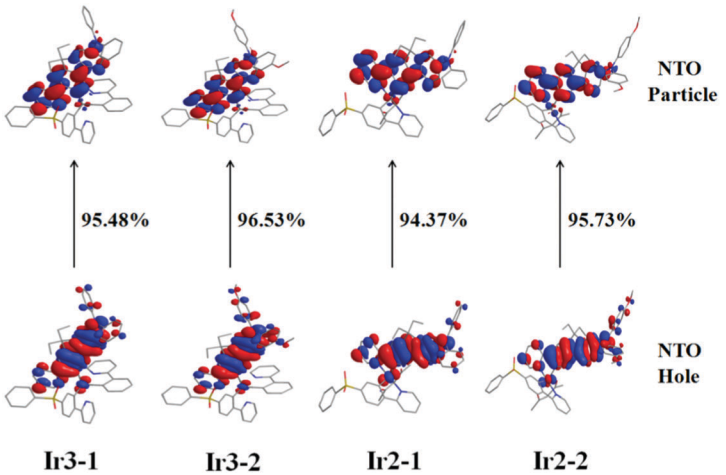

Fig. 3 Natural transition orbital patterns (isocontour value = 0.030) for $S_0 \rightarrow T_1$ excitation for these asymmetric tris-heteroleptic Ir(III) complexes based on their optimized T_1 geometries.

Table 3 NTO results for these asymmetric tris-heteroleptic Ir(III) complexes based on their optimized T_1 geometries

Complexes	NTO[a]	Contribution percentages of metal d_π orbitals and π orbitals of ligand to NTOs (%)			
Ir3-1		**Ir**	**L1**	**L3**	**ppy**
	H	4.70	94.48	0.50	0.32
	P	1.70	95.65	1.94	0.71
Ir3-2		**Ir**	**L2**	**L3**	**ppy**
	H	2.80	96.71	0.31	0.18
	P	1.60	94.43	3.09	0.88
Ir2-1		**Ir**	**L1**	**L3**	**acac**
	H	7.55	90.42	1.58	0.45
	P	2.51	95.28	1.84	0.37
Ir2-2		**Ir**	**L2**	**L3**	**acac**
	H	4.73	94.09	0.93	0.25
	P	2.41	95.06	2.17	0.36

[a] H and P represent the NTO hole and particle orbitals, respectively.

their PL spectra (Fig. 1b).[36,42] The contribution of ppy and acac to both holes and particles is less than 1%. Introducing ppy and acac to the asymmetric tris-heteroleptic Ir(III) complexes has a slight influence on the NTO distribution. So, they show similar phosphorescent spectra. Comparing the PL data of these asymmetric tris-heteroleptic Ir(III) complexes at room temperature and 77 K, no rigidochromic effect, *i.e.* blue-shift of emission wavelength at low temperature, has been observed for their major phosphorescent bands (Table 1).[14] This result also indicated the ligand-centered $^3\pi$–π^* features for the major phosphorescent bands of these asymmetric tris-heteroleptic Ir(III) complexes. Besides the dominant $^3\pi$–π^* features, the T_1 state of all the asymmetric tris-heteroleptic Ir(III) complexes should possess some MLCT features due to the contribution difference of the Ir(III) center to the NTO hole and particle orbitals (Table 3). This result can account for the structureless spectral line profile of the weaker phosphorescent band at the long wavelength region in the PL spectra of all the asymmetric tris-heteroleptic Ir(III) complexes (Fig. 1b). The obvious rigidochromic effect for this phosphorescent band also indicates their MLCT character. Hence, there is good consistency between experimental and theoretical results, indicating the validity of both the NTO results and the employed theoretical strategies.

TD-DFT calculation results have clearly indicated that the main contribution to the $S_0 \rightarrow T_1$ transitions for these asymmetric tris-heteroleptic Ir(III) complexes can be assigned to H → L+1. The contribution percentages of ligand **L1** or **L2** to L+1 are more than 85%. For **Ir2-1** and **Ir2-2**, the acac ligand accounts for less than 1% (*ca.* 0.69% and 0.73%, respectively) contribution to L+1. When the acac ligand was replaced by ppy, the contributions to L+1 from the ppy ligand are increased to 3.87% for **Ir3-1** and 7.37% for **Ir3-2**. This indicates that the introduction of the ppy ligand can decrease the electron density of the Ir centers and restrict the electron transfer from the Ir center to the other ligands to some extent, which can elevate the energy level of the LUMO and LUMO+1. So, compared with **Ir2-1** and **Ir2-2**, complexes **Ir3-1** and **Ir3-2** with three ppy-type ligands show a blue-shift effect in their phosphorescence wavelength.

Electrochemical properties

Under a nitrogen atmosphere, cyclic voltammetry (CV) measurements with ferrocene (Fc) as the internal standard had been conducted to characterize the electrochemical properties of these asymmetric tris-heteroleptic Ir(III) complexes. In the anodic scan, all the complexes can show two reversible oxidation waves (Table 4). The redox process with a lower potential (E_{pa}) can be assigned to the oxidation of the aromatic amine unit. Clearly, the first E_{pa} values of **Ir3-2** (*ca.* 0.29 V) and **Ir2-2** (*ca.* 0.26 V) are noticeably lower than those of *ca.* **Ir3-1** and **Ir2-1** (*ca.* 0.46 and 0.44 V, respectively) (Table 4). This result can be ascribed to the electron-donating methoxyl group which can definitely promote the oxidation of the aromatic amine unit in **Ir3-2** and **Ir2-2**. The second oxidation process of these asymmetric tris-heteroleptic Ir(III) complexes can be assigned to the oxidation of the Ir(III) centers.[36] This redox process is typically observed in ppy-type Ir(III) complexes.[22] Differently, in these complexes, the E_{pa}s locate in a more positive potential region (Table 4). This outcome should be due to the electron-withdrawing sulfonyl group, which can reduce the electron density on the Ir(III) centers to make them more difficult to be oxidized. All the asymmetric tris-heteroleptic Ir(III) complexes display several reduction processes. The first reduction process with E_{pc} *ca.* −2.0 V can be ascribed to the reduction of the sulfonyl group.[38,43] However, other processes are induced by the reduction of the pyridyl units in the organic ligands of the asymmetric tris-heteroleptic Ir(III) complexes.[19,20,43]

Clearly, **Ir3-1** shows a similar HOMO level to and a lower LUMO level (*ca.* −5.26 and −2.88 eV) than those of **Ir2-1** (*ca.* −5.24 and 2.81 eV, respectively). Comparing **Ir3-2** and **Ir2-2**, their HOMO and LUMO levels exhibit a similar pattern. It means that **Ir3-1** and **Ir3-2** possess a higher ability to trap electrons than **Ir2-1** and **Ir2-2**.

Electroluminescence properties

According to the literature, the EL potential of the phosphorescent emitters with the molecular configuration of **Ir3-1** and

Table 4 Redox properties of these asymmetric tris-heteroleptic Ir(III) complexes

Compound	E_{pa} (V)	E_{pc} (V)	E_{HOMO}[c] (eV)	E_{LUMO}[c] (eV)	E_g^{CV} (eV)
Ir3-1	0.46,[a] 0.69[a]	−1.92,[b] −2.19,[b] −2.78,[a] −2.95[a]	−5.26	−2.88	2.44
Ir3-2	0.29,[b] 0.74[b]	−1.84,[b] −2.17,[a] −2.52,[a] −2.80[a]	−5.09	−2.96	2.13
Ir2-1	0.44,[b] 0.61[a]	−1.99,[b] −2.21,[a] −2.53,[a] −2.80[a]	−5.24	−2.81	2.39
Ir2-2	0.26,[a] 0.58[a]	−1.94,[b] −2.18,[a] −2.51,[a] −2.75[a]	−5.06	−2.86	2.17

[a] Reversible. The value was set as $E_{1/2}$. [b] Irreversible or quasi-reversible. The value was derived from the anodic or cathodic peak potential. [c] HOMO levels are calculated according to the $E_{1/2}$ of the first reversible oxidation wave or the onset potential of the first irreversible oxidation wave, respectively. LUMO levels are derived from the onset potential of the first irreversible reduction wave.

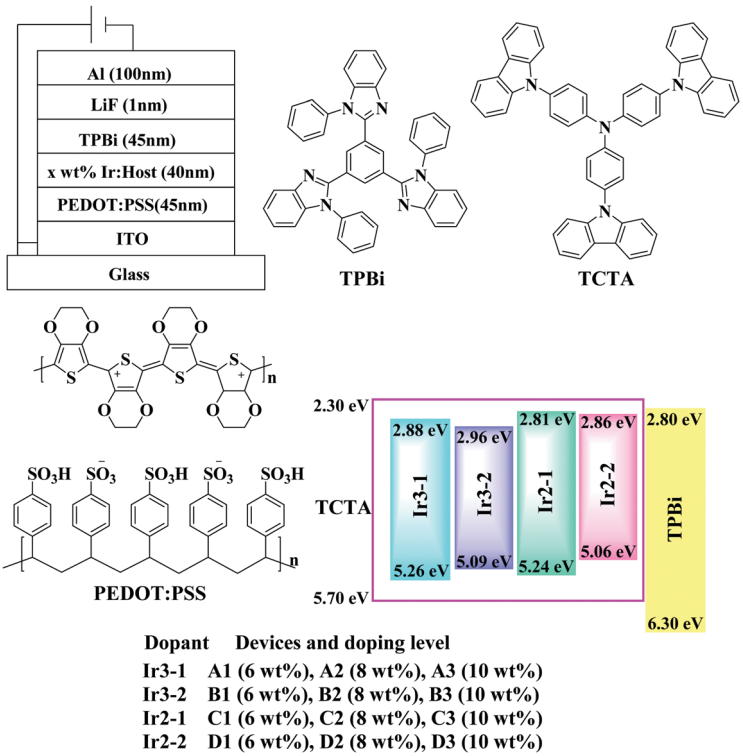

Fig. 4 Device structure of the solution-processed OLEDs together with an energy level diagram and molecular structures of the materials used in the fabricated OLEDs.

Ir3-2 has not been explored. In addition, asymmetric tris-heteroleptic Ir(III) complexes **Ir3-1** and **Ir3-2** possess higher Φ_P than **Ir2-1** and **Ir2-2** (Table 1), which is crucial for achieving high EL efficiencies.[1,6,7] On this basis, the EL performances of **Ir3-1** and **Ir3-2** have been characterized by simple solution-processed OLEDs with a configuration of ITO/PEDOT:PSS (45 nm)/Ir *x*-wt%:TCTA (40 nm)/TPBi (45 nm)/LiF (1 nm)/Al (100 nm) (Fig. 4). The spin-coated PEDOT:PSS layer acts as a hole injection layer (HIL) of the devices. Both the hole-blocking and electron-transporting functions of the OLEDs are fulfilled by the TPBi layer, while LiF serves as an electron-injection layer. Taken as references, **Ir2-1** and **Ir2-2** had also been employed to construct OLEDs with identical structures.

OLED fabrication and measurements

Pre-cleaned ITO (indium tin oxide) glass substrates were treated with ozone for 20 min. Then, poly(3,4-ethylenedioxythiophene): poly(styrenesulfonate) (PEDOT:PSS) was deposited on the surface of the ITO glass by a spin-coating method to form a 45 nm thick hole injection layer. After being cured at 120 °C for 30 min in air, the emitting layer (40 nm) was obtained by spincoating a chloroform solution of each Ir(III) complexes and 4,4′,4″-tris(carbazol-9-yl)-triphenylamine (TCTA) at various concentrations. The ITO glass was dried in a vacuum oven at 50 °C for 20 min and transferred to the deposition system for organic and metal deposition. TPBi (1,3,5-tris-(*N*-(phenyl)-benzimidazole)-benzene) (45 nm), LiF (1 nm) and an Al cathode (100 nm) were successively evaporated at a base pressure less than 10^{-6} Torr. The EL spectra and CIE coordinates were measured with a PR650 spectra colorimeter. The *J*–*V*–*L* curves of the devices were recorded by using a Keithley 2400/2000 source meter and the luminance was measured using a PR650 SpectraScan spectrometer. All the experiments and measurements were carried out under ambient conditions.

When an appropriate voltage is applied, all OLEDs can emit orange electrophosphorescence at *ca.* 560 to 570 nm (Fig. 5 and Fig. S5 in the ESI†). The EL data of these solution-processed OLEDs are summarized in Table 5. As shown in Fig. 5 and Fig. S5 in the ESI,† the EL spectral line shape of the OLEDs shows a great resemblance to the PL spectra based on these

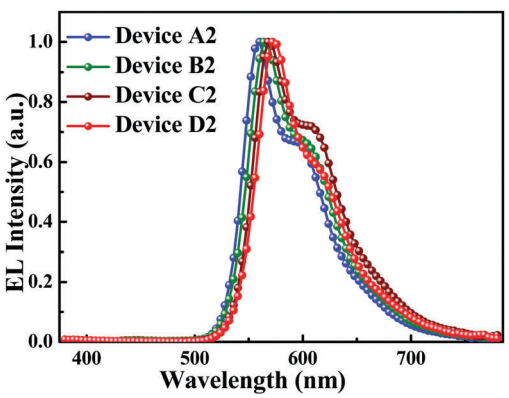

Fig. 5 EL spectra for the optimized OLEDs at *ca.* 10 V.

Table 5 EL performance of the electrophosphorescent OLEDs

Device	Dopant	$V_{turn\text{-}on}$ (V)	Luminance L_{max}[a] (cd m^{-2})	η_{ext} (%)	η_L (cd A^{-1})	η_P (lm W^{-1})	λ_{max}[d] (nm)
A1	**Ir3-1** (6.0 wt%)	3.7	32 551 (20.9)	18.6 (4.2)[a] 15.3[b] 11.8[c]	66.6 (4.2) 54.8 42.5	57.0 (3.7) 25.5 14.1	560 (0.47, 0.52)
A2	**Ir3-1** (8.0 wt%)	3.7	35 829 (18.9)	24.9 (3.7) 23.2 19.5	86.5 (3.7) 80.9 67.6	74.4 (3.7) 43.6 26.6	560 (0.49, 0.51)
A3	**Ir3-1** (10.0 wt%)	3.7	34 289 (20.4)	22.8 (4.7) 21.5 18.5	80.3 (4.7) 75.9 65.2	68.0 (3.7) 35.9 21.9	560 (0.49, 0.51)
B1	**Ir3-2** (6.0 wt%)	3.7	53 369 (19.8)	19.5 (4.1) 18.1 16.2	66.3 (4.1) 61.5 55.0	56.7 (3.7) 27.3 16.8	564 (0.50, 0.49)
B2	**Ir3-2** (8.0 wt%)	3.6	51 266 (22.9)	26.2 (4.1) 23.0 18.2	88.7 (4.1) 77.3 61.5	75.3 (3.6) 31.8 17.7	564 (0.50, 0.9)
B3	**Ir3-2** (10.0 wt%)	3.7	42 612 (21.0)	24.5 (4.2) 22.1 16.5	83.5 (4.2) 75.2 56.1	71.0 (3.7) 33.9 17.0	564 (0.51, 0.49)
C1	**Ir2-1** (6.0 wt%)	3.1	16 576 (21.4)	16.9 (3.6) 14.0 9.8	53.5 (3.6) 44.1 20.0	53.4 (3.1) 31.2 9.6	568 (0.51, 0.48)
C2	**Ir2-1** (8.0 wt%)	3.6	14 306 (21.9)	19.6 (4.1) 17.1 10.5	63.0 (4.1) 54.8 33.7	54.1 (3.6) 25.8 10.2	568 (0.53, 0.47)
C3	**Ir2-1** (10.0 wt%)	4.1	14 689 (21.9)	10.0 (4.1) 8.2 6.5	34.7 (4.1) 28.7 22.3	26.8 (4.1) 12.5 6.8	568 (0.50, 0.49)
D1	**Ir2-2** (6.0 wt%)	3.6	30 422 (21.9)	19.8 (3.6) 17.0 13.5	64.2 (3.6) 54.8 43.7	55.6 (3.6) 26.4 15.5	572 (0.53, 0.46)
D2	**Ir2-2** (8.0 wt%)	3.6	29 251 (21.9)	20.6 (4.1) 18.4 14.7	67.6 (4.1) 60.6 48.3	59.1 (3.6) 24.2 13.0	572 (0.53, 0.47)
D3	**Ir2-2** (10.0 wt%)	3.6	24 694 (21.4)	12.7 (3.6) 11.1 9.1	38.7 (3.6) 33.8 27.8	33.7 (3.6) 13.1 7.1	574 (0.54, 0.45)

[a] Maximum values of the devices. Values in the parentheses are the voltages at which they were obtained. [b] Values were collected at *ca.* 100 cd m^{-2}. [c] Values collected at *ca.* 1000 cd m^{-2}. [d] Values were collected at 10 V and CIE coordinates (x, y) are shown in parentheses.

asymmetric tris-heteroleptic Ir(III) complexes in solution (Fig. 1b), indicating that electrophosphorescence indeed originates from the triplet states of these asymmetric tris-heteroleptic Ir(III) complexes.

Current density–voltage–luminance (J–V–L) characteristics and EL efficiency–luminance curves for these solution-processed OLEDs are shown in Fig. 6, 7 and Fig. S6, S7 in the ESI.† All the OLEDs can show very high EL efficiencies despite that they had been fabricated by a convenient solution-processed method, indicating the great potential of these asymmetric tris-heteroleptic Ir(III) complexes in the EL field. The highest EL efficiencies of **Ir3-1** and **Ir3-2** have been achieved by the devices with a doping-level of *ca.* 8.0 wt% for the phosphorescent emitters, *i.e.* device **A2** for **Ir3-1** and device **B2** for **Ir3-2**

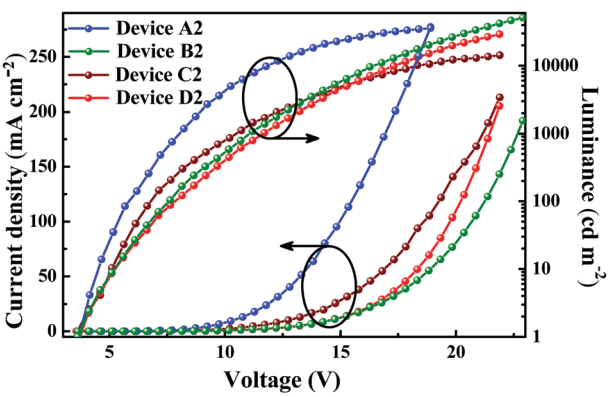

Fig. 6 Current-density–voltage–luminance (J–V–L) curves of optimized OLEDs.

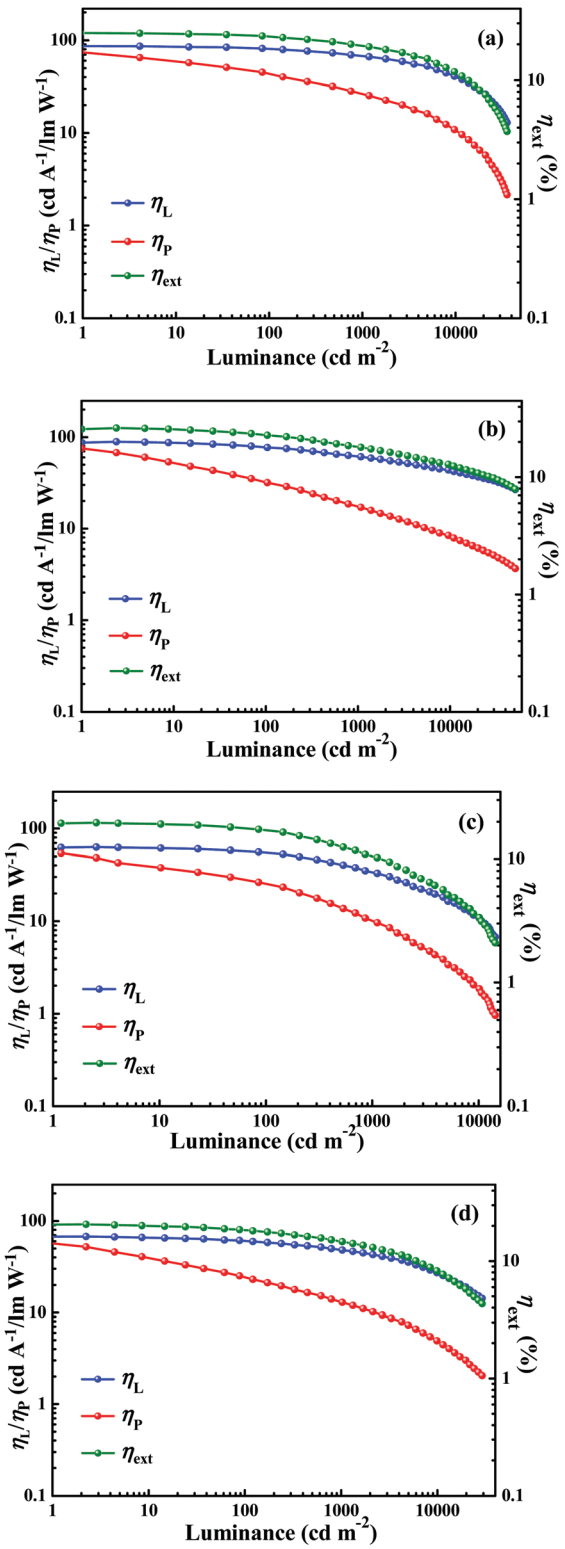

Fig. 7 Relationship between EL efficiencies and luminance of the optimized devices: (a) Device **A2**, (b) Device **B2**, (c) Device **C2** and (d) Device **D2**.

(Table 5). Device **B2** can show outstanding EL performances with a maximum external quantum efficiency (η_{ext}) of 26.2%, a maximum current efficiency (η_L) of 88.7 cd A^{-1} and a maximum power efficiency (η_P) of 75.3 lm W^{-1}. These EL results are even superior to those achieved by device **A2** with efficiencies of 24.9%, 86.5 cd A^{-1} and 74.4 lm W^{-1} (Table 5 and Fig. 7a, b). This result can be assigned to the fact that **Ir3-2** possesses a higher HOMO level (−5.09 eV for **Ir3-2** *vs.* −5.26 eV for **Ir3-1**) and a lower LUMO level (−2.96 eV for **Ir3-2** *vs.* −2.88 eV for **Ir3-1**) than **Ir3-1** (Table 4). So, **Ir3-2** can show a higher ability for trapping both holes and electrons than **Ir3-1**. According to the energy-level pattern of the emission layer of devices **A2** and **B2**, the HOMO and LUMO levels of **Ir3-1** and **Ir3-2** lie in between those of host material TCTA to make **Ir3-1** and **Ir3-2** electronically excited by direct charge-trapping in preference.[44–46] As a result, the higher ability to trap both holes and electrons associated with **Ir3-2** can enhance the recombination efficiency between holes and electrons. Accordingly, **Ir3-2** can outperform **Ir3-1** in EL devices as mentioned before (Table 5 and Fig. 7a, b).

In contrast, asymmetric tris-heteroleptic Ir(III) complexes **Ir2-1** and **Ir2-2** show noticeably lower EL efficiencies (Table 5). Optimized device **C2** with **Ir2-1** as an emitter can achieve EL efficiencies of 19.6%, 63.0 cd A^{-1} and 54.1 lm W^{-1}. Despite that device **D2** with **Ir2-2** as an emitter can exhibit enhanced EL efficiencies (20.6%, 67.6 cd A^{-1} and 59.1 lm W^{-1}) compared with device **C2**, it cannot compete with devices **B2** and **A2** (Table 5). This outcome can be ascribed to the much higher phosphorescent quantum yields (Φ_P) of **Ir3-1** (*ca.* 0.78) and **Ir3-2** (*ca.* 0.76) than those of **Ir2-1** (*ca.* 0.57) and **Ir2-2** (*ca.* 0.58) (Table 1). Based on all the EL efficiency data obtained, it can be seen clearly that the EL ability is in the order of **Ir3-2** > **Ir3-1** and **Ir2-2** > **Ir2-1** (Table 5). Obviously, introducing methoxyl groups can enhance the EL performances by furnishing a higher HOMO level, *i.e.* hole-trapping ability, of **Ir3-2** and **Ir2-2** by their electron-donating features. This conclusion can be supported by both MO patterns and TD-DFT results (Fig. 2 and Table 2).

With similar molecular configurations of **Ir2-2** and **Ir2-1**, asymmetric tris-heteroleptic Ir(III) complexes with an acac auxiliary ligand reported by our group have shown obvious advantages over their traditional symmetric counterparts.[19,21,22] Encouragingly, **Ir3-1** and **Ir3-2** can outperform **Ir2-2** and **Ir2-1** as well as their symmetric *fac*-Ir(L)$_3$ counterparts with **L1** (9.89%, 29.77 cd A^{-1} and 20.78 lm W^{-1}),[36] **L2** (40.4 cd A^{-1})[37] and **L3** (10.12%, 37.63 cd A^{-1} and 26.05 lm W^{-1}),[8] respectively. So, the exceptional EL performances associated with **Ir3-1** and **Ir3-2** not only indicate the great potential of their unique asymmetric structures in improving the EL ability of ppy-type phosphorescent emitters, but also represent important progress in the design and synthesis of new asymmetric ppy-type Ir(III) phosphorescent complexes with high EL ability.

Conclusions

In conclusion, a series of asymmetric tris-heteroleptic Ir(III) phosphorescent complexes adopting both IrLL′(acac) and IrLL′L″ chemical constitution have been successfully prepared. Critically, compared with the asymmetric analogs with IrLL′(acac)

chemical constitution, the IrLL′L″ asymmetric tris-heteroleptic Ir(III) phosphorescent complexes bearing three different ppy-type ligands can show the advantages of improved thermal stability, obviously enhanced Φ_P and higher ability for trapping both holes and electrons. Benefiting from these advantages, the IrLL′L″ asymmetric tris-heteroleptic Ir(III) phosphorescent complexes can show very impressive EL efficiencies with a maximum external quantum efficiency (η_{ext}) of 26.2%, a maximum current efficiency (η_L) of 88.7 cd A^{-1} and a maximum power efficiency (η_P) of 75.3 lm W^{-1}, much higher than the data achieved by not only their IrLL′(acac) asymmetric analogs, but also their traditional $Ir(L)_3$ symmetric counterparts. All these encouraging results not only indicate the great potential of the unique asymmetric IrLL′L″ structures bearing three different ppy-type ligands in improving the EL ability of ppy-type Ir(III) phosphorescent emitters, but also represent important progress in the design and synthesis of new asymmetric ppy-type Ir(III) phosphorescent complexes with high EL ability.

Conflicts of interest

There are no conflicts to declare.

Acknowledgements

This research was financially supported by the National Natural Science Foundation of China (21572176, 21602170), Fundamental Research Funds for the Central Universities (cxtd2015003 and xjj2016061), the China Postdoctoral Science Foundation (2015M580831 and 20130201110034), the Key Creative Scientific Research Team in Yulin City (2015cxy-25). The financial support from the State Key Laboratory for Mechanical Behavior of Materials is also acknowledged. The characterization of materials is supported by the Instrument Analysis Center of Xi'an Jiaotong University. W.-Y.W. acknowledges the financial support from the Areas of Excellence Scheme, University Grants Committee of HKSAR, China (AoE/P-03/08), Hong Kong Research Grants Council (HKBU 12304715), Hong Kong Baptist University (RC-ICRS/15-16/02) and the Hong Kong Polytechnic University.

Notes and references

1 C. Fan and C. Yang, *Chem. Soc. Rev.*, 2014, **43**, 6439–6469.
2 D. Xia, B. Wang, B. Chen, S. Wang, B. Zhang, J. Ding, L. Wang, X. Jing and F. Wang, *Angew. Chem., Int. Ed.*, 2014, **53**, 1048–1052.
3 C. H. Chang, Z. J. Wu, C. H. Chiu, Y. H. Liang, Y. S. Tsai, J. L. Liao, Y. Chi, H. Y. Hsieh, T. Y. Kuo, G. H. Lee, H. A. Pan, P. T. Chou, J. S. Lin and M. R. Tseng, *ACS Appl. Mater. Interfaces*, 2013, **5**, 7341–7351.
4 B. Tong, H.-Y. Ku, I. J. Chen, Y. Chi, H.-C. Kao, C.-C. Yeh, C.-H. Chang, S.-H. Liu, G.-H. Lee and P.-T. Chou, *J. Mater. Chem. C*, 2015, **3**, 3460–3471.
5 C. Y. Kuei, W. L. Tsai, B. Tong, M. Jiao, W. K. Lee, Y. Chi, C. C. Wu, S. H. Liu, G. H. Lee and P. T. Chou, *Adv. Mater.*, 2016, **28**, 2795–2800.
6 F. Zhao and D. Ma, *Mater. Chem. Front.*, 2017, **1**, 1933–1950.
7 X. Yang, G. Zhou and W. Y. Wong, *Chem. Soc. Rev.*, 2015, **44**, 8484–8575.
8 G. Zhou, Q. Wang, C. L. Ho, W. Y. Wong, D. Ma, L. Wang and Z. Lin, *Chem. – Asian J.*, 2008, **3**, 1830–1841.
9 Z. P. Yan, X. F. Luo, K. Liao, Z. X. Lin, Z. G. Wu, Y. H. Zhou and Y. X. Zheng, *Dalton Trans.*, 2018, **47**, 4045–4048.
10 C. Hierlinger, E. Trzop, L. Toupet, J. Ávila, M.-G. La-Placa, H. J. Bolink, V. Guerchais and E. Zysman-Colman, *J. Mater. Chem. C*, 2018, **6**, 6385–6397.
11 I. González, M. Natali, A. R. Cabrera, B. Loeb, J. Maze and P. Dreyse, *New J. Chem.*, 2018, **42**, 6644–6654.
12 H. Yu, C. Liu, Z. Yu, L. Zhang and J. Xiu, *J. Mater. Chem. C*, 2017, **5**, 3519–3527.
13 S. Lamansky, P. Djurovich, D. Murphy, F. Abdel-Razzaq, H. E. Lee, C. Adachi, P. E. Burrows, S. R. Forrest and M. E. Thompson, *J. Am. Chem. Soc.*, 2001, **123**, 4304–4312.
14 A. Tsuboyama, H. Iwawaki, M. Furugori, T. Mukaide, J. Kamatani, S. Igawa, T. Moriyama, S. Miura, T. Takiguchi and S. Okada, *J. Am. Chem. Soc.*, 2003, **125**, 12971–12979.
15 Y. Chi and P. T. Chou, *Chem. Soc. Rev.*, 2010, **41**, 638–655.
16 C. Hierlinger, D. B. Cordes, A. M. Z. Slawin, D. Jacquemin, V. Guerchais and E. Zysman-Colman, *Dalton Trans.*, 2018, **47**, 10569–10577.
17 H.-B. Han, X.-F. Ma, Z.-G. Wu and Y.-X. Zheng, *Mater. Chem. Front.*, 2018, **2**, 1284–1290.
18 D. Ma, C. Zhang, R. Liu, Y. Qiu and L. Duan, *Chem. – Eur. J.*, 2018, **24**, 5574–5583.
19 X. Xu, H. Guo, J. Zhao, B. Liu, X. Yang, G. Zhou and Z. Wu, *Chem. Mater.*, 2016, **28**, 8556–8569.
20 X. Yang, N. Sun, J. Dang, Z. Huang, C. Yao, X. Xu, C.-L. Ho, G. Zhou, D. Ma, X. Zhao and W.-Y. Wong, *J. Mater. Chem. C*, 2013, **1**, 3317–3326.
21 X. Xu, X. Yang, Y. Wu, G. Zhou, C. Wu and W. Y. Wong, *Chem. – Asian J.*, 2015, **10**, 252–262.
22 X. Xu, X. Yang, J. Dang, G. Zhou, Y. Wu, H. Li and W. Y. Wong, *Chem. Commun.*, 2014, **50**, 2473–2476.
23 E. Baranoff, B. F. E. Curchod, J. Frey, R. Scopelliti, F. Kessler, I. Tavernelli, U. Rothlisberger, M. Grätzel and M. K. Nazeeruddin, *Inorg. Chem.*, 2011, **51**, 215–224.
24 Y. Cudre, F. Franco de Carvalho, G. R. Burgess, L. Male, S. J. A. Pope, I. Tavernelli and E. Baranoff, *Inorg. Chem.*, 2017, **56**, 11565–11576.
25 M. Lepeltier, B. Graff, J. Lalevée, G. Wantz, M. Ibrahim-Ouali, D. Gigmes and F. Dumur, *Org. Electron.*, 2016, **37**, 24–34.
26 J. Langecker, O. Karg, R. Meusinger and M. Rehahn, *J. Org. Chem.*, 2018, **862**, 105–116.
27 M. C. Derosa, D. J. Hodgson, G. D. Enright, B. Dawson, C. E. Evans and R. J. Crutchley, *J. Am. Chem. Soc.*, 2004, **126**, 7619–7626.
28 Y. Tamura, Y. Hisamatsu, S. Kumar, T. Itoh, K. Sato, R. Kuroda and S. Aoki, *Inorg. Chem.*, 2017, **56**, 812–833.

29 T. D. Anthopoulos, M. J. Frampton, E. B. Namdas, P. L. Burn and I. D. W. Samuel, *Adv. Mater.*, 2004, **16**, 557–560.
30 J. H. Seo, G. Y. Park, Y. K. Kim and Y. S. Kim, *Mol. Cryst. Liq. Cryst.*, 2007, **471**, 313–323.
31 G. Y. Park, Y. Kim and Y. Ha, *Mol. Cryst. Liq. Cryst.*, 2006, **462**, 179–188.
32 M. Lepeltier, F. Dumur, B. Graff, P. Xiao, D. Gigmes, J. Lalevée and C. R. Mayer, *Helv. Chim. Acta*, 2014, **97**, 939–956.
33 Y. Tamura, Y. Hisamatsu, A. Kazama, K. Yoza, K. Sato, R. Kuroda and S. Aoki, *Inorg. Chem.*, 2018, **57**, 4571–4589.
34 Y. Hisamatsu, S. Kumar and S. Aoki, *Inorg. Chem.*, 2017, **56**, 886–899.
35 T. Hofbeck and H. Yersin, *Inorg. Chem.*, 2010, **49**, 9290–9299.
36 W. Y. Wong, G. J. Zhou, X. M. Yu, H. S. Kwok and B. Z. Tang, *Adv. Funct. Mater.*, 2006, **16**, 838–846.
37 H. Wu, G. Zhou, J. Zou, C.-L. Ho, W.-Y. Wong, W. Yang, J. Peng and Y. Cao, *Adv. Mater.*, 2009, **21**, 4181–4184.
38 G. Zhou, C.-L. Ho, W.-Y. Wong, Q. Wang, D. Ma, L. Wang, Z. Lin, T. B. Marder and A. Beeby, *Adv. Funct. Mater.*, 2008, **18**, 499–511.
39 W. R. Wadt and P. J. Hay, *J. Chem. Phys.*, 1985, **82**, 284–298.
40 P. J. Hay and W. R. Wadt, *J. Chem. Phys.*, 1985, **82**, 270–283.
41 M. J. Frisch, G. W. Trucks, H. B. Schlegel, G. E. Scuseria, M. A. Robb, J. R. Cheeseman, G. Scalmani, V. Barone, B. Mennucci, G. A. Petersson, H. Nakatsuji, M. Caricato, X. Li, H. P. Hratchian, A. F. Izmaylov, J. Bloino, G. Zheng, J. L. Sonnenberg, M. Hada, M. Ehara, K. Toyota, R. Fukuda, J. Hasegawa, M. Ishida, T. Nakajima, Y. Honda, O. Kitao, H. Nakai, T. Vreven, J. A. Montgomery, Jr., J. E. Peralta, F. Ogliaro, M. Bearpark, J. J. Heyd, E. Brothers, K. N. Kudin, V. N. Staroverov, R. Kobayashi, J. Normand, K. Raghavachari, A. Rendell, J. C. Burant, S. S. Iyengar, J. Tomasi, M. Cossi, N. Rega, J. M. Millam, M. Klene, J. E. Knox, J. B. Cross, V. Bakken, C. Adamo, J. Jaramillo, R. Gomperts, R. E. Stratmann, O. Yazyev, A. J. Austin, R. Cammi, C. Pomelli, J. W. Ochterski, R. L. Martin, K. Morokuma, V. G. Zakrzewski, G. A. Voth, P. Salvador, J. J. Dannenberg, S. Dapprich, A. D. Daniels, O. Farkas, J. B. Foresman, J. V. Ortiz, J. Cioslowski and D. J. Fox, *Gaussian 09, revision A.01*, Gaussian, Inc., Wallingford, CT, 2009.
42 X.-M. Yu, H.-S. Kwok, W.-Y. Wong and G.-J. Zhou, *Chem. Mater.*, 2006, **18**, 5097–5103.
43 J. Zhao, Y. Yu, X. Yang, X. Yan, H. Zhang, X. Xu, G. Zhou, Z. Wu, Y. Ren and W.-Y. Wong, *ACS Appl. Mater. Interfaces*, 2015, **7**, 24703–24714.
44 A. D'Aleo, M. H. Sazzad, D. H. Kim, E. Y. Choi, J. W. Wu, G. Canard, F. Fages, J. C. Ribierre and C. Adachi, *Chem. Commun.*, 2017, **53**, 7003–7006.
45 B. Liu, X.-L. Li, H. Tao, J. Zou, M. Xu, L. Wang, J. Peng and Y. Cao, *J. Mater. Chem. C*, 2017, **5**, 7668–7683.
46 B. Jiang, X. Ning, S. Gong, N. Jiang, C. Zhong, Z.-H. Lu and C. Yang, *J. Mater. Chem. C*, 2017, **5**, 10220–10224.

